Astronomy & Astrophysics manuscript no. aa
September 18, 2019

Spectroscopic Analysis of Fornax Dwarf Galaxies

I. Kinematics & Kinematic Scaling Relation

F. S. Eftekhari[1,2], R. Peletier[1], N. Scott[3], and S. Mieske[2]

[1] Kapteyn Astronomical Institute, Postbus 800, 9700 AV Groningen, The Netherlands
[2] European Southern Observatory, Alonso de Córdova 3107, Vitacura, Santiago, Chile
[3] ??

Received October 1, 2019; accepted March 15, 2020

ABSTRACT

Context.

Aims.

Methods.

Results.

Key words.

1. Introduction

Still after decades of studying dwarf galaxies, the formation and evolution of these objects is considered an active debate. Over the past few years, alongside improvement of observation the idea behind the lifeline of these faint and small objects had become clearer (e.g. Ryś et al. 2013, Toloba et al. 2015, Venhola et al. 2018). However, the need for more detailed and precise data to close this debate is still on the table. Thus with high resolution multiplexing deep-SAMI data cubes and statistically significant sample of dEs in Fornax cluster, we've started a new journey to collect new information from kinematics, chemical composition and structure of these faint objects.
Why studying these faint objects is important, how we approached these questions, and what new results and clues are accomplished are the questions which are going to be investigated in this research. This is the first paper of the Spectroscopic Analysis of Fornax Dwarf Galaxies series, and is dedicated to kinematic studies of dwarf early-type galaxies within Fronax galaxy cluster. The section 1 will continue to inspect why dwarf galaxies received lots of attention in the past decades. Section 2 will be dedicated to the details of our data and its comparison to previous observations. In section 3 & 4, we'll explain the methods that have been used and our results respectively. Finally, Section 5 will present the discussion and conclusions.

1.1. Why dwarf galaxies?

Different theories and ideas about the formation history of the big zoo of galaxies have been developed in the past decades. For galaxies inside clusters one of the main mechanisms governing their formation and evolution is environmental effects such as ram-pressure stripping (Lin & Faber 1983), harassment (Moore et al. 1998), or starvation (Larson et al. 1980). An ideal source to investigate the role of environment are dwarf galaxies, since they have low mass and low density and thus are more vulnerable to environmental effects.

1.2. What we know about dwarfs?

Dwarf galaxies despite their plain appearance and smooth light distribution have complex characteristics (Lisker 2006), which indicate the influence of environment in their past.
Spatial distribution of dwarfs: early-type dwarf galaxies (dEs) outnumber all other galaxy types in dense environment, like clusters, while late-type low-luminosity galaxies are the dominant population in the fields (e.g. Dressler 1980, Sandage et al. 1985, and Ferguson & Bingelli 1994).
Inner structure vs. local density of dEs: A substructure-density relation is seen in early-type dwarf galaxies, such that dEs with blue center or no nucleus are mostly found in low-density cluster regions, dEs with disks in intermediate-density regions, and nucleated dEs in high-density regions of the cluster (Ferguson & Sandage 1989, van den Bergh 1986, and Lisker et al. 2007).
Color vs. local density of dEs: dEs in higher density regions are redder compared to other regions (Lisker et al. 2008).
Kinematics vs. local density of dEs: pressure supported dEs are mostly found in high density regions of cluster, whereas in lower density regions like outskirts the angular momentum of dEs increases and dEs are largely rotationally supported. Also fast rotators in the outer part of the cluster rotate faster than fast rotators in the inner parts of the cluster (Toloba et al. 2009, van Zee et al.

2004a, and Toloba et al. 2015).
Dwarf galaxies's formation history is another key to the formation and evolution of galaxies; whether dwarf galaxies are the descendants in hierarchical structure formation (Moore et al. 1999) and were created by gravitational collapse like other galaxies (Kauffmann & White 1993), or whether they were formed at later epoch from late-type low-luminosity star forming galaxies by environmental effects (Boselli & Gavazzi 2006, Gavazzi et al. 2013, and Boselli & Favazzi 2014). The answer to these questions could be achieved by pursuing the behaviour and location of these galaxies inside galaxy physical parameter space.
Surface brightness profile: logarithm of the S*é*rsic index of both dwarfs and giant early-type galaxies linearly increases with central surface brightness and magnitude, but SB profiles of dEs are less steep than massive ellipticals (Gavazzi et al. 2005, Graham & Guzm*á*n 2013, and Young & Currie 1994).
Color magnitude relation: there is no gap seen between dwarfs and giant ellipticals in color magnitude profile (e.g. Ferrarese et al. 2006, Janz & Lisker 2009, and Misgeld et al. 2008&2009).
Fundamental plane: inside fundamental plane it's been seen that dEs are offset with respect to the plane of early-type galaxies (Toloba et al. 2012 and Rijcke et al. 2015).
Disky substructure: disk-like structures have been seen in fast rotators and dEs in the outer regions of cluster, also they have rotation curves similar to those of late-type galagixes (Toloba et al. 2015 and Toloba et al. 2009).
Star formation: As the galay's luminosity decreases the duration of star formation increases (Gavazzi et al. 2002), also H_β absorption index increases from giants to dwarfs as luminosity and velocity dispersion decreases (Poggianti et al. 2001 and Geha et al 2003).

2. Data

The SAMI Fornax project started in 2015 with the Sydney-AAO Multi-Object Integral-field (SAMI) spectrograph on the Anglo-Australian Telescope (AAT), with aim of studying the origin and the inner workings of dwarf galaxies inside Fornax cluster. As results of total ?? allocated nights in 2015B, 2016B and 2018B, we have ?? dwarf galaxies, ?? giant elliptical galaxies with good spectra.
SAMI is an integral-field spectrograph equipped by 13 fiber-based IFUs called hexabundles, and 26 pluggable sky fibers (Bryant et al. 2014). Each hexabundle with a field-of-view of 15″ diameter, is made of 61 1.6-arcsecond optical fibers. These hexabundles have physical size <1 mm, with a filling fraction of 73 per cent and together with sky fibers each fits into pre-drilled holes in a field plate. The plug plate with about 1 degree field-of-view is installed a the AAT's Prime Focus Camera top end and so hexabundle's face is placed at the focal plane of the telescope. To study structure of low-mass galaxies such as dEs in Fornax cluster, high resolution spectra and high S/N were needed. With 1500V gratings in blue and 100R gratings in red, our data has resolution of 5100 (FWHM = 1.0Å) in blue ($\sim 4660 - 5430A^o$) and 4300 (FWHM = 1.6Å) in red ($6250 - 7350A^o$). Which means ambitiously reaching around 25 km/s and 30 km/s velocity dispersion in blue and red respectively. And with fourteen 30 minutes exposure times for each field gaining high S/N became possible. Moreover compared to single IFU instruments we can simultaneously observe 12 galaxies and one calibration star which significantly increases the observation rate.

Most of the previous surveys are long slit, which make them susceptible to aperture effects. While Integral Field Spectroscopy spatially resolves each galaxy and gives different spectra at different parts of the galaxy. Also current IFU surveys (e.g. SAMI Galaxy Survey, MANGA) are not useful for the study of dEs due to sensitivity, effective spatial resolution and most importantly spectral resolution limitations. A comparison between theses projects can be seen in table 1.

Table 1: Projects on Dwarf Galaxies

Survey	No.	λ	FWHM	Cluster	Telescope
SAMI_Fornax	60	4660-5430 (B) 6250-7350 (R)	1.0 1.6	Fornax	SAMI@AAO
SAURON	12	4760-5300	3.9	Virgo	WHT@ING
SMACKED	10	4600-5600	1.6	Virgo	INT@ING
	26	4200-5000 (B) 5500-6700 (R)	1.4 3.2	Virgo	WHT@ING
	3	4500-5600	2.7	Virgo	VLT@ESO
MAGPOP	4	3500-7100 (B) 8000-9100 (R)	1.6 3.2	Virgo	WHT&INT@ING TNG@INAF

Our sample was selected based on Fornax Deep Survey (FDS). Considering the aim was to study star formation and evolution of dEs within Fornax cluster, the primary survey targets are FDS galaxies that cover $-18 < M_r < -14.5$ and $17 < \mu_r < 23$, also in different environments from center of the cluster to outside of its virial radius (4° or 1.4 Mpc) such as dEs in Fornax A. In total around 100 galaxies were observed, but we had to eliminate about half of them since they were too faint and had noisy spectra that couldn't be fitted by pPXF even when their light was integrated. This resulted in a complete sample of 48 early-type galaxies, mostly dwarf elliptical galaxies which are listed in table ?? **[table of galaxies to be added]**. In the following section we describe the methods used for extraction of kinematics of these objects.

3. Methods

To extract stellar kinematics or stellar population (3rd paper) from absorption-line spectra of galaxies we used the Penalized Pixel-Fitting method (pPXF). We extracted stellar kinematics and stellar population (3rd paper) from absorption-line spectra of our galaxies by using the penalised Pixel Fitting (pPXF) routine of Cappellari & Emsellen (2004). pPXF basically is a maximum penalized likelihood approach in pixel space, with the aim of finding an optimal temple with the minimum template-galaxy mismatch errors. It finds the best-fitting linear combination of input stellar templates by convolving them with the line-of-sight velocity distribution of the input galaxy's spectra, and then the best-fitting parameters are determined by non-linear chi-squared minimization in pixel space (logarithmically binned in wavelength). The best match for SAMI-Fornax's wavelength range and spectral resolution is single-age single-metallicity population models of PÉGASE-HR (Le Borgne et al. 2004). PÉGASE-HR is the result of applying the PÉGASE.2 code on ÉLODIE. ÉLODIE is a high resolution stellar library of 1959 spectra for 1503 stars with R=10 000 at lambda=550 nm.
During spectra fitting with pPXF we also include an additive Legendre polynomial of 6th degree and a multiplicative Legendre polynomial of 10 order to correct the template continuum shape during the fit. They're in account for ??. For all of the galaxies we measure the Gauss-Hermite moments of the LOSVD up to h_4, even though at our minimum S/N ?? the data is unable to constrain all of the V, σ, h_3, and h_4 parameters.In pPXF one can also fit the gas emission lines together with the stellar kinematics and population. But for the current work since not all

Table 2

FCC name	FDS name	year	RA (deg)	DEC (deg)	R_e (arcsec)	M_r (mag)	μ_r ($mag/arcsec^2$)	ϵ	n	g-r (mag)
FCC213	FDS11_DWARF003	2016	54.620899	-35.450439	114.88±8.41	-23.02±0.08	20.70±0.23	0.92	5.80	0.84
FCC167	FDS11_DWARF006	2016	54.115009	-34.976017	44.49±2.49	-22.01±0.06	19.18±0.17	0.59	2.88	0.73
FCC219	FDS11_DWARF166	2016	54.716400	-35.593323	26.15±1.09	-22.00±0.05	18.45±0.13	0.87	3.60	0.82
FCC184	FDS11_DWARF001	2016	54.237602	-35.506592	73.56±5.68	-21.84±0.09	20.91±0.24	0.93	7.47	0.87
FCC276	FDS6_DWARF001	2018	55.580955	-35.392532	110.84±11.36	-21.62±0.11	21.72±0.32	0.70	7.85	0.73
FCC29	FDS25_DWARF000	2018	50.984844	-36.464443	43.82±2.72	-21.56±0.07	19.92±0.19	0.81	5.43	0.76
FCC179	FDS12_DWARF003	2016	54.192539	-35.999268	74.62±6.79	-21.23±0.10	20.84±0.29	0.48	6.86	0.73
FCC147	FDS16_DWARF001	2016	53.819111	-35.226257	29.51±1.67	-21.08±0.06	19.75±0.17	0.98	5.39	0.75
FCC83	FDS19_DWARF000	2018	52.645653	-34.853939	55.35±4.74	-20.82±0.10	20.87±0.27	0.61	6.81	0.80
FCC193	FDS11_DWARF000	2016	54.298901	-35.746105	15.53±0.74	-20.34±0.05	18.67±0.15	0.66	3.09	0.75
FCC153	FDS15_DWARF002	2016	53.87944	-34.447021	23.15±1.66	-19.62±0.08	18.63±0.22	0.15	1.62	0.74
FCC177	FDS10_DWARF000	2016	54.197838	-34.739735	28.81±2.51	-19.34±0.10	20.01±0.27	0.26	1.66	0.69
FCC249	FDS13_DWARF000	2018	55.175434	-37.510769	7.13±0.30	-19.21±0.05	18.54±0.12	0.98	3.47	0.81
FCC190	FDS11_DWARF005	2016	54.287319	-35.195053	16.23±1.07	-19.19±0.07	20.28±0.20	0.92	1.81	0.85
FCC277	FDS6_DWARF002	2018	55.594924	-35.154098	11.44±0.68	-18.82±0.07	19.39±0.18	0.58	1.89	0.65
FCC143	FDS16_DWARF002	2016	53.746666	-35.171089	9.81±0.56	-18.66±0.06	19.63±0.17	0.85	4.34	0.74
FCC235	FDS11_DWARF519	2016	55.041069	-35.629093	42.30±5.54	-18.57±0.14	22.64±0.42	0.68	0.85	0.34
FCC301	FDS7_DWARF000	2018	56.264900	-35.972668	7.60±0.41	-18.34±0.06	18.89±0.16	0.54	2.12	0.72
FCC263	FDS5_DWARF000	2018	55.385574	-34.888752	16.47±1.38	-18.28±0.09	20.51±0.26	0.48	1.37	0.48
FCC37	FDS25_DWARF241	2018	51.289337	-36.365185	33.89±4.35	-18.17±0.14	22.56±0.41	0.68	1.09	0.45
FCC33	FDS26_DWARF003	2018	51.243237	-37.009613	16.89±1.51	-18.07±0.10	20.50±0.28	0.37	1.18	0.66
FCC285	FDS7_DWARF360	2018	55.760147	-36.273357	32.65±4.32	-17.97±0.15	22.78±0.42	0.74	1.22	0.37
FCC182	FDS11_DWARF279	2016	54.226295	-35.374714	9.67±0.66	-17.89±0.08	20.50±0.21	0.96	2.43	0.81
FCC136	FDS16_DWARF159	2016	53.622837	-35.546459	17.50±1.72	-17.77±0.11	21.78±0.31	0.85	2.14	0.78
FCC106	FDS15_DWARF417	2018	53.198673	-34.238728	10.65±0.87	-17.42±0.09	20.44±0.26	0.49	2.18	0.68
FCC202	FDS11_DWARF235	2015	54.527325	-35.439911	13.28±1.25	-17.34±0.11	21.21±0.30	0.59	1.67	0.73
FCC113	FDS15_DWARF107	2018	53.279419	-34.805576	18.92±2.35	-17.04±0.14	22.45±0.39	0.69	1.19	0.48
FCC222	FDS11_DWARF283	2015	54.805500	-35.371410	16.10±1.86	-16.97±0.13	22.44±0.36	0.89	1.35	0.69
FCC100	FDS16_DWARF417	2018	52.948479	-35.051388	19.77±2.56	-16.96±0.14	22.72±0.41	0.76	1.46	0.71
FCC203	FDS10_DWARF189	2016	54.538200	-34.518761	16.04±1.88	-16.90±0.13	21.97±0.37	0.55	1.46	0.66
FCC135	FDS15_DWARF384	2016	53.628445	-34.297371	14.72±1.68	-16.82±0.13	21.70±0.36	0.47	1.58	0.64
FCC207	FDS11_DWARF396	2015	54.580185	-35.129124	9.59±0.92	-16.59±0.11	21.63±0.30	0.83	1.54	0.66
FCC245	FDS11_DWARF458	2018	55.140991	-35.022888	14.52±1.78	-16.50±0.14	22.72±0.39	0.92	1.51	0.62
FCC252	FDS11_DWARF069	2018	55.209988	-35.748455	11.13±1.21	-16.41±0.12	22.25±0.34	0.94	1.21	0.69
FCC300	FDS7_DWARF326	2018	56.249588	-36.319752	20.82±3.23	-16.38±0.17	23.37±0.49	0.72	1.14	0.67
FCC266	FDS6_DWARF455	2018	55.422161	-35.170265	6.91±0.58	-16.35±0.09	21.23±0.26	0.89	1.17	0.66
FCC46	FDS22_DWARF244	2018	51.604301	-37.127785	8.51±0.82	-16.31±0.11	21.35±0.30	0.64	0.98	0.49
FCC188	FDS11_DWARF155	2015	54.268906	-35.590149	12.20±1.45	-16.26±0.13	22.64±0.38	0.96	1.00	0.69
FCC211	FDS11_DWARF339	2015	54.589504	-35.259689	6.58±0.58	-16.11±0.10	21.17±0.27	0.75	1.66	0.64
FCC164	FDS12_DWARF367	2016	54.053589	-36.166451	9.95±1.13	-16.00±0.13	21.85±0.36	0.55	1.47	0.63
FCC306	FDS7_DWARF310	2018	56.439095	-36.346100	7.26±0.71	-15.91±0.11	21.33±0.31	0.59	0.90	0.32
FCC253	FDS13_DWARF042	2018	55.230301	-37.837627	10.92±1.36	-15.83±0.14	22.35±0.39	0.62	1.13	0.71
FCC274	FDS6_DWARF208	2015	55.571922	-35.540737	12.05±1.62	-15.75±0.15	23.12±0.43	0.96	1.26	0.58
FCC298	FDS6_DWARF098	2018	56.185070	-35.683716	6.97±0.71	-15.62±0.11	21.73±0.32	0.71	1.19	0.62
FCC264	FDS6_DWARF170	2015	55.382313	-35.589550	10.27±1.34	-15.51±0.14	22.06±0.41	0.40	1.05	0.58
FCC195	FDS10_DWARF014	2016	54.347183	-34.900108	12.78±1.92	-15.44±0.16	22.92±0.48	0.54	1.06	0.66
FCC250	FDS13_DWARF258	2018	55.184971	-37.408268	9.22±1.27	-15.06±0.15	22.97±0.44	0.76	0.84	0.72
FCC178	FDS10_DWARF302	2016	54.202728	-34.280102	11.26±1.76	-15.02±0.17	23.37±0.50	0.71	1.24	0.58
FCC134	FDS15_DWARF223	2016	53.590393	-34.592522	6.52±0.84	-14.60±0.14	22.36±0.41	0.57	0.81	0.48
FCC51	FDS21_DWARF129	2018	51.776043	-36.636787	4.45±0.52	-14.15±0.13	22.21±0.37	0.70	0.96	0.64

of the galaxies have emission lines, we avoid regions with emission lines by simply masking them to gain the best fitting spectra. Another interesting feature in this method is regularization which is used to reduce the noise in the recovery of the stellar population parameters and more importantly it attaches a physical meaning to the output weights assigned to the best-fitting template in term of the star formation history (SFH) or metallicity distribution of each galaxy. This feature was important in stellar population of our galaxies (SAMI-Fornax paper 3).

In case of galaxies with emission lines we avoid regions with emission lines by simply masking them, which is also possible by gas feature within the latest version of pPXF. Galaxies with prominent emission lines are ??. Moreover, We computed the uncertainties by (100 realizations) Monte Carlo simulations. In each loop the best-fitted spectra is disturbed by random spectra convolved by the sigma of the difference between original and best-fitted template spectra.

For kinematic maps to have accurate measured velocity and velocity dispersion we require high S/N. This can be achieved by Voronoi binning algorithm (Cappellari & Copin 2003), which starts from the central pixels with highest S/N and accretes closes neighboring pixels to reach the target S/N. We chose $(S/N)_{min} = 15$ for velocity dispersion maps and $(S/N)_{min} = 10$ for Velocity maps, which is a comprise between assurance of the reliability of extracted kinematics and spatial resolution of images.

In order to check the accuracy of our results, we compared them with Toloba et al. 2011 study on dwarf galaxies which can be seen in plot ??. Our measurement show ...

4. Scaling Relations

To understand the origin of dwarf galaxies, the role of environment in evolution of these low-mass stellar systems and also their dark matter content, we analyze their fundamental kinematic scaling relations. Manifolds of galaxy properties such as the Faber-Jackson, the fundamental Plane (FP), the color-velocity dispersion relation, and etc.

4.1. Faber Jackson

One of the first discoveries in early-type galaxies was that their stellar velocity dispersion correlates with their luminosity (Faber & Jackson 1967). This 2 dimensional realtion $L \propto \sigma^{\alpha}$, Faber-Jackson relation is in fact a projection of Fundamental Plane. It has been shown that the slope of this relations gets shallower as it goes to fainter objects (Davies et al. 1983). In Fig.1 we go down to faint low-mass galaxies of $M \sim 10^{7.4} M_{\odot}$ color coded by surface brightness within effective radius. **[what we see?]**

4.2. Fundamental Plane

The empirical Fundamental plane which is a bivariate relation (Brosche 1973, Dressler et al. 1973 and Djorgovski & Davis 1987) between R_e (the half light ration radius of the galaxy), I_e (the mean surface brightness within Re in flux units), and σ (the galaxy internal velocity dispersion), is an indication of galaxies being in virial equilibrium $R_e \propto \sigma^2 I_e^{-1} (M/L)^{-1}$ (Binney & Tremaine 2008). By assuming the mass-to-light ratio M/L to be a power-law function of σ and I_e, the physical quantities can be replaced by observables and the edge-on view of FP will be simplified to

$$log(R_e) = \alpha log(\sigma) + \beta < \mu_e > + \gamma \tag{1}$$

where $< \mu_e >$ is the mean surface brightness in $mag/arcsec^2$ defined as $-2.5log(I_e) + cte$. The derived coefficients of FP (Bernardi et al 2003) are not exactly the same as the predicted ones from the virial theorem . This deviation of coefficients (tilt) also tightness of the plane have always been some of the keys for better understanding evolution of galaxies, their structure and stellar population, or even dark matter content of galaxies (Renzini & Ciotti 1993, , Borriello et al. 2003). **[some examples of α and β from literature]**
In this projection of FP (eq. 1) which is commonly used all distance-dependent quantities, velocity dispersion and surface brightness, are collected in one side. But we will also study the other projection $log(\sigma) = \alpha' log(R_e) + \beta' < \mu_e > + \gamma'$, which here dependent variables R_e and μ_e are in one side. For calculation of error bars in this projection we also need covariance matrix between R_e and μ_e.

The common way to find this best fitted plane in the three dimensional space of ($logR_e$, μ_e, $log\sigma$) is least absolute deviation orthogonal fit (e.g. Jørgensen et al. 1996, Falcón-Barroso et la. 2011, and Cappellari et al. 2013). The advantage of least absolute deviation to the famous least-square deviation is that by treating all parameters symmetrically it's relatively insensitive to few outliers. In this method the residuals perpendicular to the plane are

$$D = \frac{|log(R_e) - \alpha log(\sigma) - \beta < \mu_e > - \gamma|}{\sqrt{\alpha^2 + \beta^2 + 1}} \tag{2}$$

Also the uncertainties of coefficients are derived by bootstrap procedure **[must be done]**. Even though the FP in Fig.2 is derived from least-absolute deviation method, the FP we got from least-square deviation is quite similar since we didn't have any significant outliers in SAMI-Fornax data sample.
In integrated galaxy specra, lines broadening can be caused by both velcoity dispersion and the galaxy's rotational velocity. The effect of V_{rot} will more prominent in elongated rotational galaxies such as FCC177 and FCC153. Without considering their rotational velocity they will deviate from FP, so we didn't include them in FP fitting.
[when bring up the comparisons with literature such as Toloba et al. 2011?]

... But since our galaxy is concentrated on elliptical galaxies and so dispersion supported σ is the measure of the mass of each galaxy... **?** ... Replacing velocity dispersions of our giant galaxies with Fornax3D results did not show prominent difference in FP. So we will stick with SAMI-fornax results for both giant and dwarf galaxies, as standard properties calculated from different methods are tended to have different systematic errors. ...

4.3. Fundamental Plane in the κ-space

For more transparent analysis of FP, Bender et al. (1992) defined a new coordinate system by a simple orthogonal coordinate transformation of the 3 dimensional space of ($logR_e$, $logI_e$, $log\sigma^2$) as following

$$\kappa_1 \equiv (log\sigma_0{}^2 + logr_e)/\sqrt{2} \tag{3}$$

$$\kappa_2 \equiv (log\sigma_0{}^2 + 2logI_e - logr_e)/\sqrt{6} \tag{4}$$

$$\kappa_3 \equiv (log\sigma_0{}^2 - logI_e - logr_e)/\sqrt{3} \tag{5}$$

By defining luminosity and mass as $L = c_1 I_e r_e{}^2$ and $M = c_2 \sigma_0{}^2 r_2$, each of the coordinates will have a specific physical meaning. κ_1 being representative of galaxies size or logarithm of mass, κ_2 being representative of the logarithm of M/L and κ_3 being representative of the logarithm of $(M/L) I_e{}^3$. Also in κ coordinate system $\kappa_1 - \kappa_2$ and $\kappa_1 - \kappa_3$ projections correspond to face-on and edge-on viwe of FP respectively.
In Fig.3 we see distribution of SAMI-Fornax galaxies in kappa space, together with Toloba et al. (2011) sets of dwarf galaxies within Virgo galaxies. Their observations were done in V and K band , so we needed to transform them to r band first by using transformations between magnitude systems. **[what we see?]**

4.4. Dynamical Mass

Variety in dark matter fraction of dEs can be accounted as one of the reasons for deviation of dEs from FP (e.g. Reda et al. 2005) or even FP tilt (e.g. Cappellari et al. 2006, and Graves & Faber 2010). We measure dynamical mass and dark matter fraction of our galaxies within SAMI field-of-view following Wolf et al. 2010.
Not considering the difference between radial and tangential velocity dispersion weakens the accuracy of conclusions about structure and formations of galaxies. This becomes more important when calculating dynamical mass of a galaxy by only having its 2d observed radial properties. Wolf et al. 2010 using the spherical Jeans equation showed that within r_3 radius this difference is insignificant. r_3 is where the log-slope of the 3D tracer density profile is -3, and for dispersion supported galaxies it is

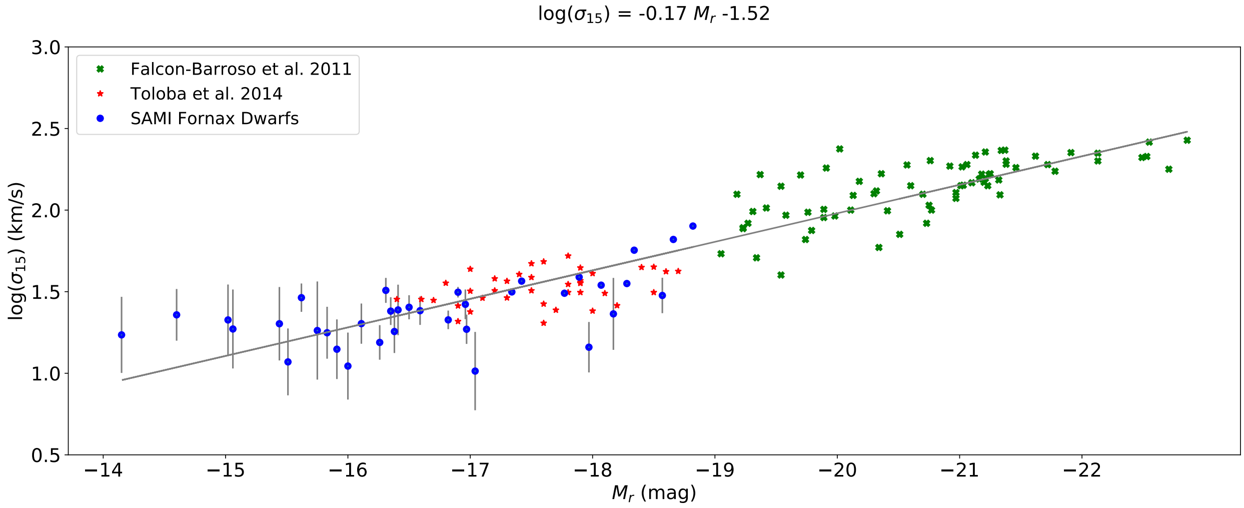

Fig. 1: Faber Jackson Relation

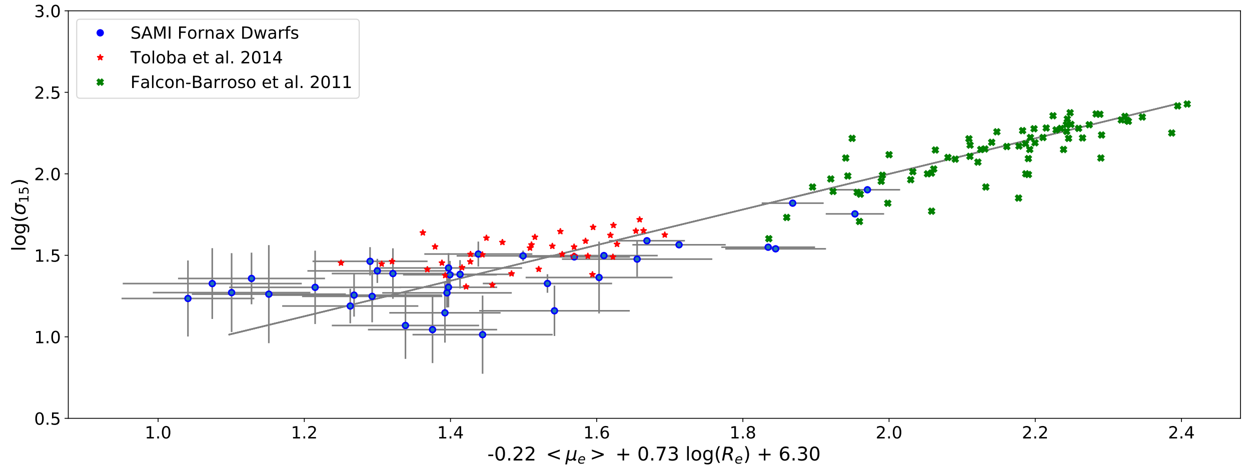

Fig. 2: Fundamental plane in two different Projections

close to the 3D half-light radius $r_{1/2}$. So the dynamical will be defined as:

$$M_{1/2} \simeq 930(\frac{{\sigma_{los}}^2}{km^2 s^{-2}})(\frac{R_e}{pc})M_\odot \tag{6}$$

where R_e is the 2D projected half-light radius and σ_{los} is the line-of-sight velocity dispersion. In Fig.4 we expand the relationship between $M_{1/2}$ and the half-light luminosity $L_{1/2} = 0.5L$ for elliptical and dwarf elliptical galaxies. The first thing we see is that our galaxies connect well with the brighter dwarfs of Toloba et al (2014) and elliptical galaxies of Falcon-Barroso et al. 2010 both within Virgo cluster also the Local Group dwarfs from Wolf et al (2010). This means that the dark matter properties of these dwarfs in clusters are the same as in the Local Group, implying that the dark matter distribution inside the galaxies is not affected by the cluster environment. Moreover, as emphasized in Wolf et al 2010 and Zaritsky et al. 2006 dEs are sitting at the minimum of the parabola relation between dynamical half-light mass-to-light ratio and velocity dispersion. Position of the minimum and its corresponding mass scales are important as it's the turnover point between two different star formation scenario of bright and faint systems. Three different power-law regimes / two different regimes? what they mean?

4.5. Color vs. σ

To have a look at stellar population and ?? of these objects, one can have a look at color versus velocity dispersion relation of them Fig.6
[Discussion]

5. Phase-Space Diagrams

6. Conclusions

Acknowledgements.

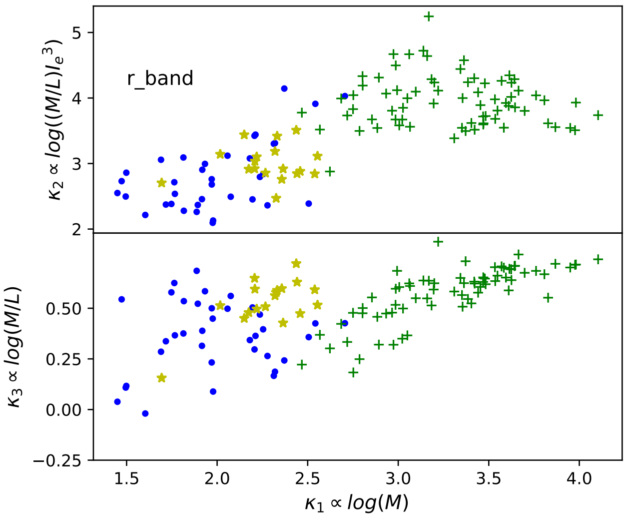

Fig. 3: FP in κ space

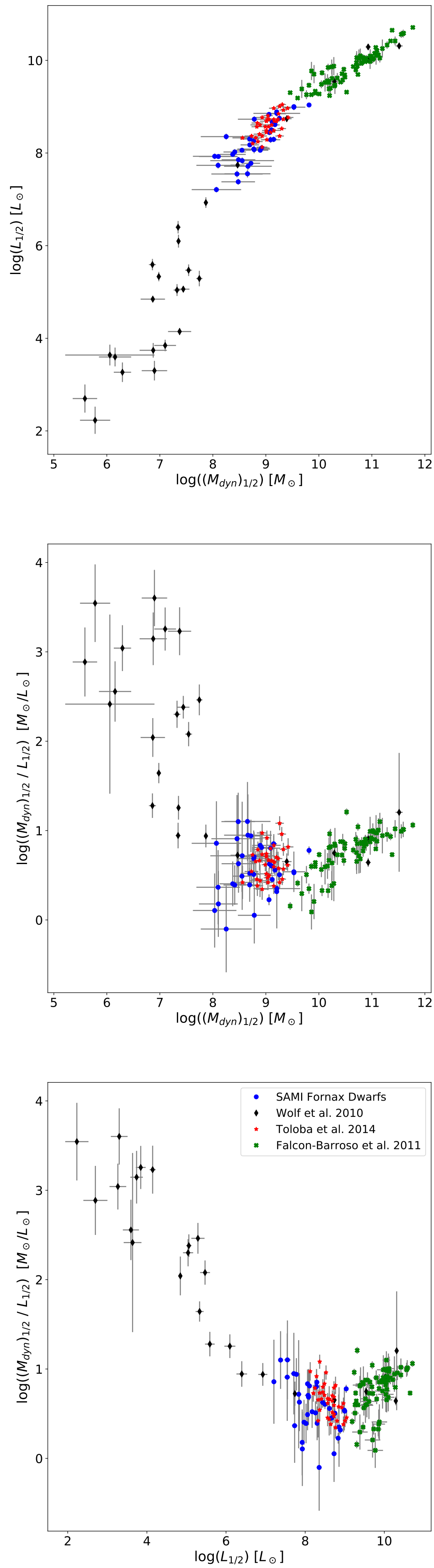

Fig. 4: Dynamical Mass vs. Luminosity ratio **[info box must be added]**

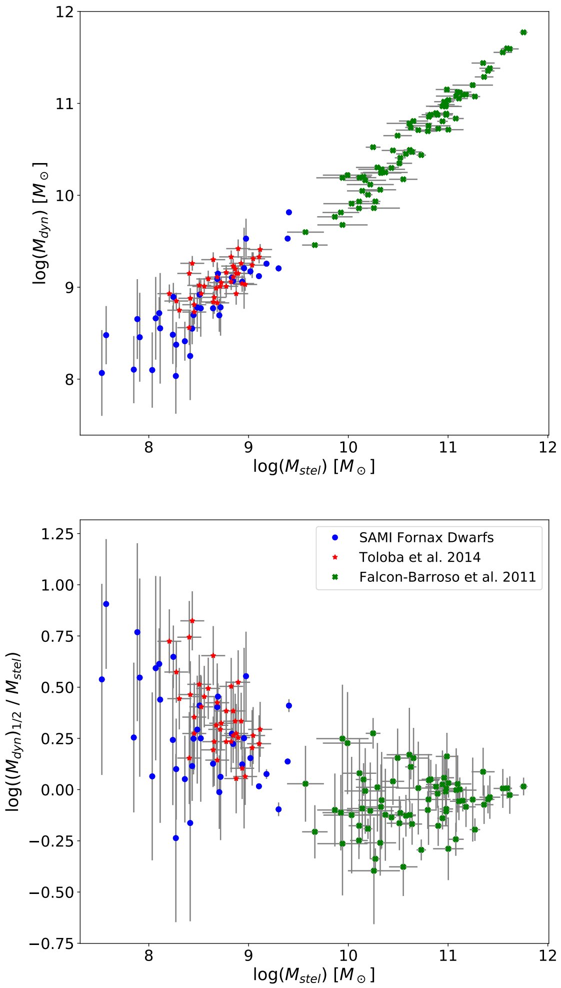

Fig. 5: Stellar Mass vs. Luminosity ratio **[info box must be added]**

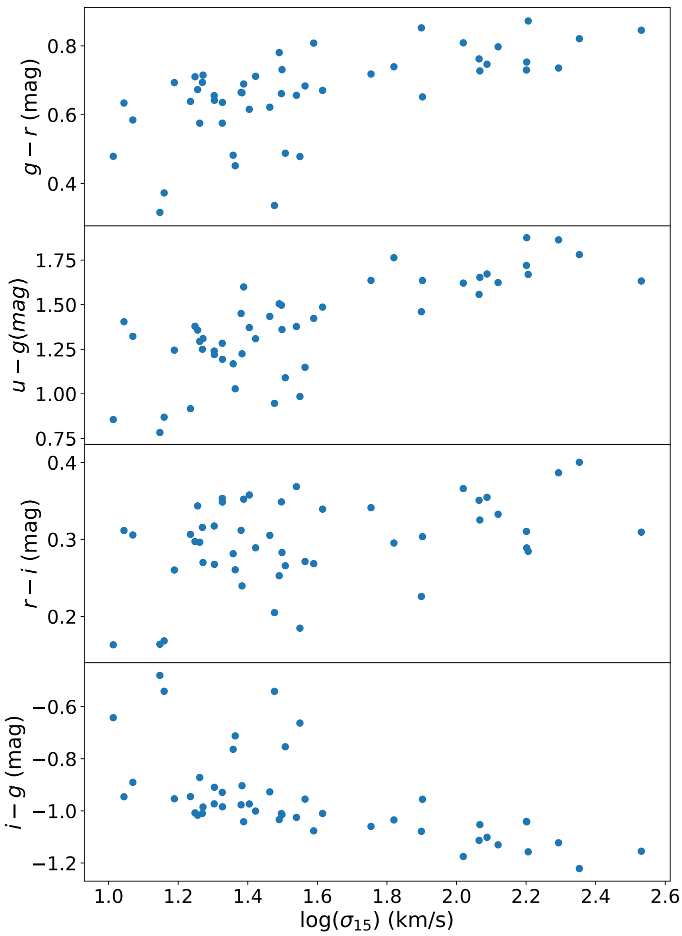

Fig. 6: Color vs. Dispersion

Table 3

FCC	$\log(M_*/M_\odot)_r$	σ(km/s)	$\log(L_{r,1/2}(L_{Sun})$	$\log(M_{dyn,1/2})(M_{Sun})$	$(M/L)_r(M_{Sun}/L_{Sun})$
213	11.28±0.0020	339.81±6.48	10.76±0.032	12.07±0.016	20.33±1.68
167	10.89±0.0019	143.40±1.21	10.35±0.024	10.91±0.007	3.55±0.20
219	10.96±0.0018	154.30±3.28	10.35±0.020	10.74±0.018	2.44±0.15
184	10.81±0.0021	143.40±1.70	10.29±0.036	11.12±0.010	6.87±0.59
276	10.65±0.0025	123.30±0.64	10.20±0.044	11.17±0.004	9.37±0.95
29	10.69±0.0020	116.12±1.01	10.18±0.0280	10.72±0.007	3.47±0.2321
179	10.5091±0.0024	70.0000±1.4730	10.0470±0.0400	10.5115±0.0183	2.9145±0.2951
147	10.4283±0.0020	131.1000±1.4951	9.9870±0.0240	10.6537±0.0099	4.6418±0.2775
83	10.4017±0.0023	102.8000±0.5972	9.8830±0.0400	10.7156±0.0051	6.8017±0.6315
193	10.1979±0.0020	95.3000±1.3667	9.6910±0.0200	10.0978±0.0125	2.5520±0.1385
249	9.8011±0.0020	103.8000±0.5797	9.2390±0.0200	9.8340±0.0049	3.9355±0.1865
190	9.6728±0.0022	74.6200±7.8886	9.2310±0.0280	9.9045±0.0918	4.7157±1.0424
277	9.4690±0.0022	80.1700±2.9007	9.0830±0.0280	9.8149±0.0314	5.3947±0.5229
143	9.4560±0.0022	62.3100±1.0189	9.0190±0.0240	9.5293±0.0142	3.2382±0.2079
235	9.0386±0.0034	29.9744±7.4942	8.9830±0.0560	9.5283±0.2172	3.5104±1.8128
301	9.3652±0.0022	48.7400±1.8700	8.8910±0.0240	9.2051±0.0333	2.0611±0.1949
263	9.0004±0.0027	28.0000±1.3586	8.8670±0.0360	9.0595±0.0421	1.5579±0.1988
37	9.0192±0.0033	23.1160±11.7317	8.8230±0.0560	9.2064±0.4408	2.4178±2.4738
33	9.2439±0.0027	34.6622±0.9357	8.7830±0.0400	9.2558±0.0235	2.9707±0.3172
285	8.7834±0.0035	14.4437±5.1387	8.7430±0.0600	8.7817±0.3090	1.0933±0.7925
182	9.1682±0.0024	39.2000±0.4939	8.7110±0.0320	9.1205±0.0109	2.5675±0.1999
136	9.0824±0.0028	30.9298±1.5543	8.6630±0.0440	9.1723±0.0437	3.2308±0.4611
106	8.8965±0.0027	36.6946±1.2047	8.5230±0.0360	9.1050±0.0285	3.8201±0.4040
202	8.9093±0.0028	31.5052±1.0090	8.4910±0.0440	9.0684±0.0278	3.7799±0.4531
113	8.4790±0.0035	10.3114±5.6974	8.3710±0.0560	8.2520±0.4799	0.7605±0.8461
222	8.7708±0.0033	18.6047±3.8464	8.3430±0.0520	8.6946±0.1796	2.2469±0.9672
100	8.7505±0.0035	26.4483±5.5318	8.3390±0.0560	9.0893±0.1817	5.6275±2.4634
203	8.7570±0.0033	31.3815±2.3254	8.3150±0.0520	9.1470±0.0644	6.7931±1.2943
135	8.7083±0.0032	21.2401±2.7843	8.2830±0.0520	8.7707±0.1139	3.0742±0.8861
207	8.5125±0.0030	24.1795±4.8484	8.1910±0.0440	8.6972±0.1742	3.2080±1.3269
245	8.5729±0.0035	25.3773±4.3179	8.1550±0.0560	8.9193±0.1478	5.8126±2.1153
252	8.5849±0.0032	24.4416±8.7130	8.1190±0.0480	8.7712±0.3096	4.4903±3.2396
300	8.5498±0.0041	18.0232±5.4663	8.1070±0.0680	8.7786±0.2634	4.6953±2.9414
266	8.4988±0.0028	24.0355±4.7049	8.0950±0.0360	8.5497±0.1700	2.8491±1.1401
46	8.3101±0.0031	32.2014±5.6714	8.0790±0.0440	8.8942±0.1530	6.5342±2.3950
188	8.4255±0.0035	15.4514±3.7701	8.0590±0.0520	8.4128±0.2119	2.2585±1.1348
211	8.3387±0.0029	20.1410±5.7160	7.9990±0.0400	8.3749±0.2465	2.3763±1.3664
164	8.3351±0.0034	11.0678±5.2301	7.9550±0.0520	8.0344±0.4105	1.2008±1.1439
306	7.9136±0.0033	14.0366±5.9076	7.9190±0.0440	8.1039±0.3656	1.5310±1.2980
253	8.3048±0.0036	17.7121±6.4887	7.8870±0.0560	8.4832±0.3182	3.9471±2.9364
274	8.1779±0.0039	18.2740±12.6537	7.8550±0.0600	8.5531±0.6014	4.9908±6.9460
298	8.1686±0.0033	29.0552±5.8133	7.8030±0.0440	8.7182±0.1738	8.2262±3.3956
264	8.0985±0.0038	11.7375±5.5398	7.7590±0.0560	8.0992±0.4100	2.1890±2.0855
195	8.1332±0.0041	20.1151±10.4218	7.7310±0.0640	8.6621±0.4500	8.5328±8.9308
250	7.9732±0.0040	18.6780±10.4047	7.5790±0.0600	8.4559±0.4839	7.5320±8.4557
178	7.9490±0.0043	21.2195±10.6095	7.5630±0.0680	8.6535±0.4343	12.3176±12.4674
134	7.6366±0.0040	22.8041±8.3158	7.3950±0.0560	8.4788±0.3167	12.1280±8.9825
51	7.5933±0.0037	17.1884±9.2307	7.2150±0.0520	8.0673±0.4665	7.1178±7.6923